Magnetic Field Measurement

Steven A. Macintyre
Macintyre Electronic Design

Magnetic field strength is measured using a variety of different technologies. Each technique has unique properties that make it more suitable for particular applications. These applications can range from simply sensing the presence or change in the field to the precise measurements of a magnetic field's scalar and vector properties. A very good and exhaustive fundamental description of both mechanical and electrical means for sensing magnetic fields can be found in Lion [1]. Less detailed but more up-to-date surveys of magnetic sensor technologies can be found in [2, 3]. It is not possible to adequately describe all of these technologies in the space available in a Handbook. This chapter concentrates on sensors that are commonly used in magnetic field measuring instruments.

As shown in Figure 48.1, magnetic field sensors can be divided into vector component and scalar magnitude types. The vector types can be further divided into sensors that are used to measure low fields (<1 mT) and high fields (>1 mT). Instruments that measure low fields are commonly called *magnetometers*. High-field instruments are usually called *gaussmeters*.

The induction coil and fluxgate magnetometers are the most widely used vector measuring instruments. They are rugged, reliable, and relatively less expensive than the other low-field vector measuring instruments. The fiber optic magnetometer is the most recently developed low-field instrument. Although it currently has about the same sensitivity as a fluxgate magnetometer, its potential for better performance is large. The optical fiber magnetometer has not yet left the laboratory, but work on making it more rugged and field worthy is under way. The superconducting quantum interference device (SQUID) magnetometers are the most sensitive of all magnetic field measuring instruments. These sensors operate at temperatures near absolute zero and require special thermal control systems. This makes the SQUID-based magnetometer more expensive, less rugged, and less reliable.

The Hall effect device is the oldest and most common high-field vector sensor used in gaussmeters. It is especially useful for measuring extremely high fields (>1 T). The magnetoresistive sensors cover the middle ground between the low- and high-field sensors. Anisotropic magnetoresistors (AMR) are currently being used in many applications, including magnetometers. The recent discovery of the giant

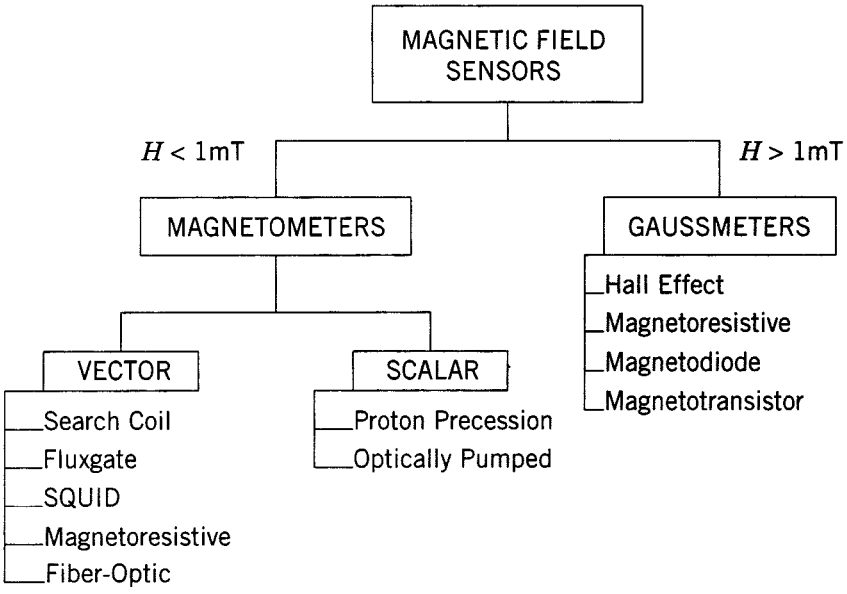

FIGURE 48.1 Magnetic field sensors are divided into two categories based on their field strengths and measurement range: magnetometers measure low fields and gaussmeters measure high fields.

TABLE 48.1 Field Strength Instrument Characteristics

Instrument	Range (mT)	Resolution (nT)	Bandwidth (Hz)	Comment
Induction coil	10^{-10} to 10^{6}	Variable	10^{-1} to 10^{6}	Cannot measure static fields
Fluxgate	10^{-4} to 0.5	0.1	dc to 2×10^{3}	General-purpose vector magnetometer
SQUID	10^{-9} to 0.1	10^{-4}	dc to 5	Highest sensitivity magnetometer
Hall effect	0.1 to 3×10^{4}	100	dc to 10^{8}	Best for fields above 1T
Magnetoresistance	10^{-3} to 5	10	dc to 10^{7}	Good for mid-range applications
Proton precession	0.02 to 0.1	0.05	dc to 2	General-purpose scalar magnetometer
Optically pumped	0.01 to 0.1	0.005	dc to 5	Highest resolution scalar magnetometer

magnetoresistive (GMR) effect, with its tenfold improvement in sensitivity, promises to be a good competitor for the traditional fluxgate magnetometer in medium-sensitivity applications.

The proton (nuclear) precession magnetometer is the most popular instrument for measuring the scalar magnetic field strength. Its major applications are in geological exploration and aerial mapping of the geomagnetic field. Since its operating principle is based on fundamental atomic constants, it is also used as the primary standard for calibrating magnetometers. The proton precession magnetometer has a very low sampling rate, on the order of 1 to 3 samples per second, so it cannot measure fast changes in the magnetic field. The optically pumped magnetometer operates at a higher sampling rate and is capable of higher sensitivities than the proton precession magnetometer, but it is more expensive and not as rugged and reliable.

Table 48.1 lists various magnetic field strength instruments and their characteristics.

48.1 Magnetic Field Fundamentals

An understanding of the nature of magnetic fields is necessary in order to understand the techniques used for measuring magnetic field strength. The most familiar source of a magnetic field is the bar

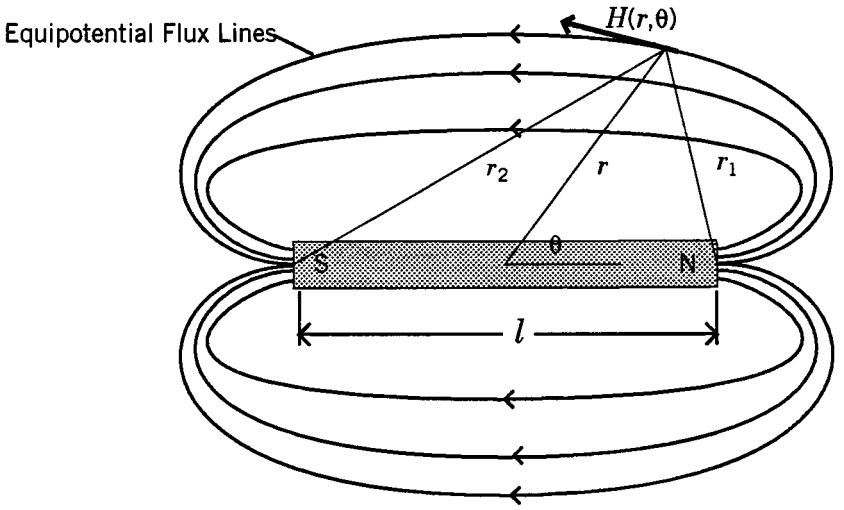

FIGURE 48.2 Magnets produce magnetic fields. A magnetic field is a vector quantity with both magnitude and direction properties.

magnet. The field it produces is shown in Figure 48.2. Magnetic field is a vector quantity; that is, it has both a magnitude and a direction. The field of a bar magnet or any other magnetized object, when measured at a distance much greater than its longest dimension, is described by Equation 48.1:

$$\vec{H} = \frac{3\left(\vec{m} \times \hat{a}_r\right)\hat{a}_r - \vec{m}}{r^3} \tag{48.1}$$

where $\hat{a}_r$ is a unit vector along *r*, *r* is the distance between the magnetic field source and the measurement point, and $\vec{m}$ is called the magnetic dipole moment. The derivation of this equation can be found in many textbooks on electromagnetics. This is a very convenient equation for estimating the field produced by many magnetized objects.

The strength or intensity of a magnetized object depends on the density of its volume-distributed moments. This intensity is called its magnetization *M*, which is defined as the moments per unit volume:

$$\vec{M} = \frac{\vec{m}}{volume} \tag{48.2}$$

Like magnetic field, magnetization is a vector quantity. Magnetization is a material property that can arise from internal magnetic sources as well as be induced by an external magnetic field.

There is a third magnetic vector $\vec{B}$ called magnetic induction or flux density. In free space, magnetic field and magnetic induction are proportional to one another by a constant factor μ_0.

$$\vec{B} = \mu_0 \vec{H} \tag{48.3}$$

Things are different in matter. Equation 48.4 describes the relationship among the magnetic field, magnetic induction, and magnetization vectors in matter:

$$\vec{B} = \mu_0\left(\vec{H} + \vec{M}\right) \tag{48.4}$$

In this case, the magnetic induction and the magnetic field vectors do not necessarily have the same direction. Some materials have anisotropic magnetic properties that make these two vectors point in different directions. The magnetization vector can consist of permanent and induced magnetization components. The permanent magnetization vector does not depend on the presence of an external field. The induced magnetization vector does depend on an external magnetic field and only exists while the inducing field is present.

Magnetic materials can be loosely classified as magnetically "soft" or magnetically "hard." In a magnetically hard material, the permanent magnetization component dominates (a magnet is an example). Magnetization in a soft magnetic material is largely induced and is described by the following equation:

$$\vec{M} = \chi \vec{H} \tag{48.5}$$

where χ is called the material's magnetic susceptibility. In an isotropic material (magnetic properties are not direction dependent), χ is a scalar quantity, and the magnetization and field vectors are proportional and aligned. In anisotropic material (magnetic properties depend on direction), χ is a tensor represented by a 3×3 matrix; therefore, the magnetization vector magnitude and direction depend on the direction and strength of the inducing field. As a result, the magnetization vector will not always align with the magnetization inducing field vectors. Equation 48.5 can be modified for magnetically "soft" material to the following:

$$\vec{B} = \mu_0 \left(1 + \chi\right) \vec{H} = \mu_0 \mu \vec{H} \tag{48.6}$$

where μ is called the relative permeability of the material.

A magnetized object with a magnetic moment $\vec{m}$ will experience torque $\vec{T}$ in the presence of a uniform magnetic field $\vec{H}$. Equation 48.7 expresses this relationship.

$$\vec{T} = \vec{m} \times \vec{H} \tag{48.7}$$

Torque is the cross-product of the magnetic moment and field vectors. The magnitude equation is:

$$T = mH \sin\theta \tag{48.8}$$

where θ is the angle between the direction of $\vec{m}$ and $\vec{H}$.

There is an intimate relationship between electric and magnetic fields. Oersted discovered that passing a current through a wire near a compass causes the compass needle to rotate. The compass was the first magnetic field strength sensor. Faraday found that he could produce an electric voltage at the terminals of a loop of wire if he moved a magnet near it. This led to the induction or search coil sensor.

Magnetic fields are produced by the flow of electric charge (i.e., electric currents). In effect, a magnetic field is a velocity-transformed electric field (through a Lorentz transformation). Current flowing through a straight wire, a loop of wire, or a solenoid will also produce a magnetic field as illustrated in Figure 48.3.

Units are always a problem when dealing with magnetic fields. The Gaussian cgs (centimeter, gram, and second) system of units was favored for many years. Since $\mu_0 = 1$ in the cgs system, magnetic field and flux density have the same numeric value in air, and their units (oerstedt for field and gauss for flux density) are often indiscriminately interchanged. This has led to great confusion. The cgs system has now been replaced by the International System of Units (SI). The SI system uses, among others, the meter (m), kilogram (kg), second (s) and ampere (A) as the fundamental units. Payne [4] gives a very good explanation of the differences between these systems of units as they relate to magnetic fields. Table 48.2 summarizes the relationships between the two systems of units.

The SI system of units is used throughout this chapter.

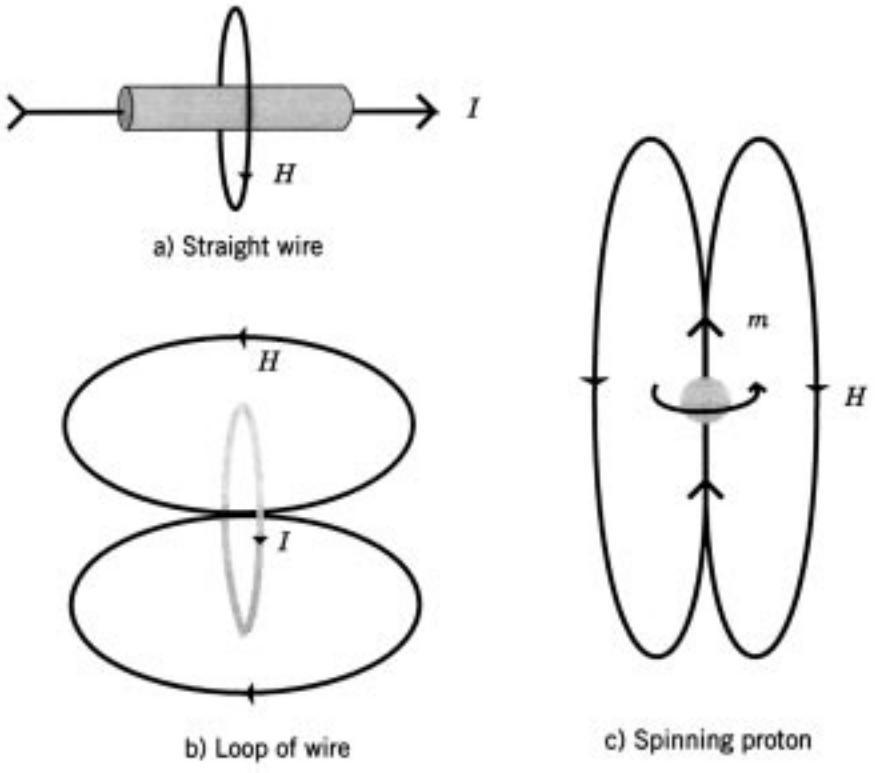

FIGURE 48.3 Magnetic fields are also produced by electric currents.

TABLE 48.2 Factors for Converting from cgs to SI Magnetic Field Units

Description	Symbol	SI unit	Gaussian cgs unit	Multiply by
Magnetic induction	B	Tesla	gauss	10^4
Magnetic field strength	H	A m^{-1}	oerstedt (oe)	$4\pi \times 10^{-3}$
Magnetization	M	A m^{-1}	emu m^3	10^{-3}
Magnetic dipole moment	m	A m^2	emu	10^3
Magnetic flux	ϕ	Weber (Wb)	maxwell	10^8
Magnetic pole strength	p	A m	emu	
Permeability of free space	μ_0	H m^{-1}	$4\pi \times 10^{-7}$	1

48.2 Low-Field Vector Magnetometers

The Induction Coil Magnetometer

The induction or search coil, which is one of the simplest magnetic field sensing devices, is based on Faraday's law. This law states that if a loop of wire is subjected to a changing magnetic flux, ϕ, through the area enclosed by the loop, then a voltage will be induced in the loop that is proportional to the rate of change of the flux:

$$e(t) = -\frac{d\phi}{dt} \tag{48.9}$$

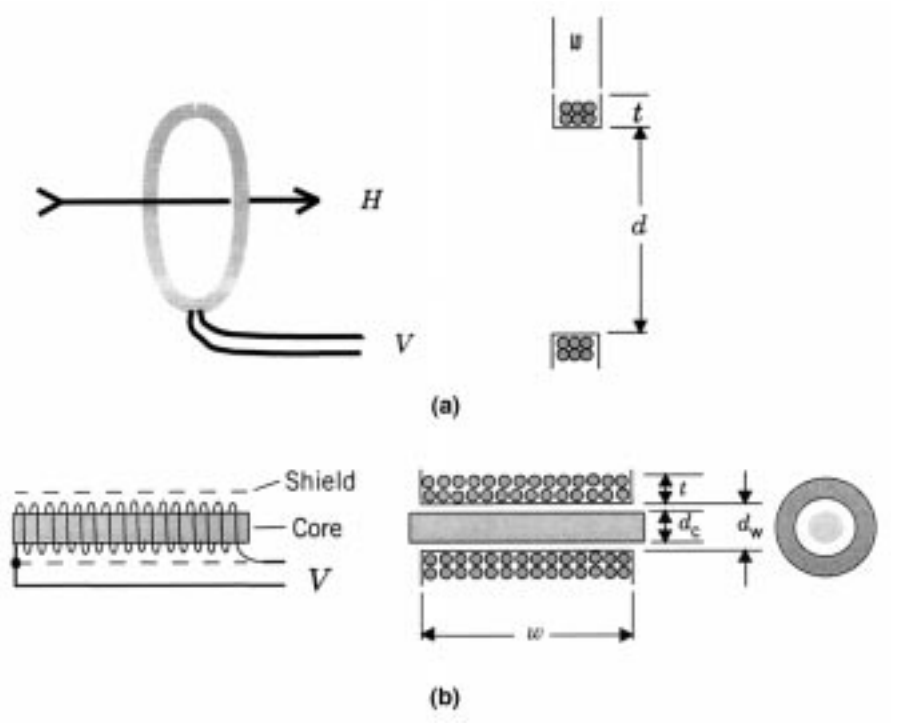

FIGURE 48.4 Induction or search coil sensors consist of a loop of wire (or a solenoid), which may or may not surround a ferromagnetic core. (a) Air core loop antenna; (b) solenoid induction coil antenna with ferromagnetic core.

Since magnetic induction $\vec{B}$ is flux density, then a loop with cross-sectional area $\vec{A}$ will have a terminal voltage:

$$e(t) = -\frac{\mathrm{d}\left(\vec{B} \bullet \vec{A}\right)}{\mathrm{d}t} \tag{48.10}$$

for spatially uniform magnetic induction fields.

Equation 48.10 states that a temporal change in $\vec{B}$ or the mechanical orientation of $\vec{A}$ relative to $\vec{B}$ will produce a terminal voltage. If the coil remains fixed with respect to $\vec{B}$, then static fields cannot be detected; but if the loop is rotated or the magnitude of $\vec{A}$ is changed, then it is possible to measure a static field. The relationship described by Equation 48.10 is exploited in many magnetic field measuring instruments (see [1]).

Figure 48.4 shows the two most common induction coil configurations for measuring field strength: the air core loop antenna and the rod antenna. The operating principle is the same for both configurations. Substituting $\mu_0\mu_e H(t)$ for B in Equation 48.10 and, assuming the loop is stationary with respect to the field vector, the terminal voltage becomes:

$$e(t) = -\mu_0\mu_e nA\frac{\mathrm{d}H(t)}{\mathrm{d}t} \tag{48.11}$$

where n is the number of turns in the coil, and μ_e is the effective relative permeability of the core. The core of a rod antenna is normally constructed of magnetically "soft" material so one can assume the flux density in the core is induced by an external magnetic field and, therefore, the substitution above is valid. With an air (no) core, the effective relative permeability is one. The effective permeability of an induction

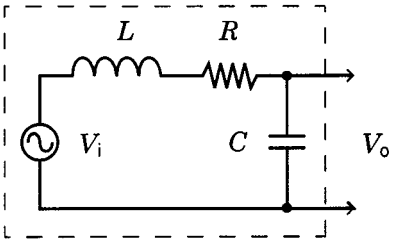

FIGURE 48.5 The induction coil equivalent circuit is a frequency-dependent voltage source in series with an inductor, resistor, and lumped capacitor.

coil that contains a core is usually much greater than one and is strongly dependent on the shape of the core and, to some extent, on the configuration of the winding.

Taking the Laplace transform of Equation 48.11 and dividing both sides by H, one obtains the following transfer function $T(s)$ for an induction coil antenna:

$$T(s) = -\mu_0\mu_e nAs = -Ks \quad \left(\text{VmA}^{-1}\right) \tag{48.12}$$

where $E(s) = T(s)\,H(s)$, $E(s)$ and $H(s)$ are the Laplace transforms of $e(t)$ and $H(t)$, and s is the Laplace transform operator. Inspection of Equation 48.12 reveals that the magnitude of the coil voltage is proportional to both the magnitude and frequency of the magnetic field being measured. The coil constant or sensitivity of the loop antenna is:

$$K = \mu_0\mu_e nA \quad \left(\text{VsmA}^{-1}\right) \tag{48.13}$$

Figure 48.5 is the equivalent circuit for an induction coil antenna. The actual voltage measured at the terminals of the loop is modified by the inductance L, resistance R, and the distributed stray and shield capacitances represented by the lumped capacitor C. These circuit parameters depend on the geometry of the core, coil, and winding.

The electrostatic shield made of nonmagnetic material shown in Figure 48.4 is an important element in the design of an induction coil. It prevents coupling of electric fields into the coil, thereby assuring that the signal seen at the coil terminals is only that due to a magnetic field. The shield should not be placed too close to the winding since it contributes to coil capacitance and noise.

The Air Core Loop Antenna

The air core loop antenna consists of a circular or rectangular loop containing one or more turns of wire and no magnetic core. The diameter of the loop is usually much greater than the dimensions of the winding cross-section. The sensitivity of a circular loop antenna with a winding inside diameter d and rectangular cross-section is approximately:

$$K = \mu_0 n\pi\frac{d^2}{4}\left[1 + 2\left(\frac{t}{d}\right) + \frac{3}{4}\left(\frac{t}{d}\right)^2\right] \tag{48.14}$$

where t is the thickness of the winding and n is the number of turns.

The resistance of the coil is:

$$R = 4n\frac{d}{d_w^2}\left(1 + \frac{t}{d}\right)\rho\ \Omega \tag{48.15}$$

where d_w is the diameter of the bare wire and ρ is its resistivity in Ω m (1.7×10^{-8} Ω m for copper).

The inductance of the coil is more difficult to compute since it depends heavily on the geometry of the coil. Those who are interested in computing very accurate inductance values for a wide variety of coil shapes should consult [5]. Equation 48.16 is a general expression that gives a good approximation for the inductance of a circular air core coil.

$$L = \mu_0 n^2 \pi \left(\frac{\bar{d}}{2}\right)^2 \frac{k}{w} \quad \text{H} \tag{48.16}$$

where w is the width of the winding, $\bar{d}$ is the average diameter, and k is Nagaoka's constant:

$$k = \frac{1}{1 + 0.45\frac{\bar{d}}{w} + 0.64\frac{t}{\bar{d}} + 0.84\frac{t}{w}} \tag{48.17}$$

The distributed capacitance of the coil contributes the most to the overall antenna capacitance. The parasitic capacitances can usually be ignored. Equation 48.18 can be used to estimate the distributed capacitance of a coil.

$$C_d = \left[\frac{\varepsilon_w \varepsilon_1}{\varepsilon_w t_1 + \varepsilon_1 t_w}\right] \frac{0.018544 \bar{d} w \left(n_1 - 1\right)}{n_1^2} \tag{48.18}$$

where ε_w is the dielectric constant of the wire insulation, ε_l is the dielectric constant of the interlayer insulation if any, t_w is the thickness of the wire insulation, t_l is the thickness of the interlayer insulation, and n_l is the number of layers. Adding a second layer to a single-layer coil significantly increases the capacitance but, as the number of layers increases, the capacitance decreases.

The air core loop antenna is particularly useful for measuring magnetic fields with frequencies from 100 Hz to several megahertz. Because it has a linear response to magnetic field strength, it has virtually no intermodulation distortion. On the negative side, the size of the sensor can get quite large for applications that require high sensitivities at low frequencies.

The Rod Antenna

The rod antenna is a good alternative to an air core loop antenna. It is smaller in size than a loop antenna with the same sensitivity, and it can be designed to operate at lower frequencies. Unfortunately, its response to magnetic field strength can be nonlinear and the core adds noise.

Figure 48.4(b) is a typical configuration for a rod antenna. It is basically a solenoid with a magnetic core. The core can have a circular or rectangular cross-section and can be made from a ferrite, a nickel-iron alloy, an amorphous metal glass alloy, or some other material with high relative permeability. The winding can be wound directly on the core or on a form through which the core is inserted. Insulation is sometimes placed between layers of the winding to reduce distributed capacitance. An electrostatic shield is placed around the winding to attenuate any electric field coupling into the signal. The shield has a gap that runs the length of the winding. This prevents circulating currents in the shield from attenuating the magnetic field within the coil.

The most common rod antenna configuration is a core with a circular cross-section and a tightly coupled winding that runs most of the length of the core. The sensitivity of the rod antenna is computed by substituting μ_e in Equation 48.13 with the following:

$$\mu_e = 1 + \left(\frac{d_c}{d + t}\right)^2 \left(\bar{\mu} - 1\right) \tag{48.19}$$

TABLE 48.3 Demagnetizing Factors, N for Rods and Ellipsoids Magnetized Parallel to Long Axis

Dimensional ratio (length/diameter)	Rod	Prolate ellipsoid	Oblate ellipsoid
0	1.0	1.0	1.0
1	0.27	0.3333	0.3333
2	0.14	0.1735	0.2364
5	0.040	0.0558	0.1248
10	0.0172	0.0203	0.0696
20	0.00617	0.00675	0.0369
50	0.00129	0.00144	0.01472
100	0.00036	0.000430	0.00776
200	0.000090	0.000125	0.00390
500	0.000014	0.0000236	0.001576
1000	0.0000036	0.0000066	0.000784
2000	0.0000009	0.0000019	0.000392

where d_c is the core diameter and $\bar{\mu}$ is the core average effective permeability. The core effective or apparent permeability depends on its geometry and initial permeability, as well as the winding length relative to the core length. A rod becomes magnetized when a magnetic field is applied to it. In response, a magnetic field is created within the rod that opposes the externally applied field and reduces the flux density. The demagnetizing field is proportional to the magnetization and the net field H in the core is:

$$H = H' - NM \tag{48.20}$$

where H' is the applied external field, N is the demagnetizing factor, and M is the magnetization. The apparent relative permeability of a core is the ratio of the flux density B in the middle of the core to the flux density in air:

$$\frac{B}{\mu_0 H'} = \mu_a = \frac{\mu_i}{1 + N\left(\mu_i - 1\right)} \tag{48.21}$$

where μ_i is the initial relative permeability of the core material. Initial relative permeability is the slope of the B–H magnetization curve near zero applied field for a closed magnetic path.

The value of N is shape dependent. As the length-to-diameter ratio m of a rod increases, N decreases and the apparent relative permeability approaches the initial permeability. Table 48.3, which is reproduced from [6], lists demagnetizing factors for a rod, prolate ellipsoid (cigar shape), and oblate ellipsoid (disk shape).

Equation 48.22 can be used to approximate the value of N for cylindrical rods with $m > 10$ and $\mu_i > 1000$:

$$N = \frac{2.01 \times \log_{10} m - 0.46}{m^2} \tag{48.22}$$

The apparent permeability of a rod with a small m and large μ_i is almost exclusively determined by m alone. Table 48.4 lists the magnetic properties of several ferromagnetic materials that can be used to construct a core.

Bozorth [7] found that the apparent permeability of a rod is not constant throughout the length of the rod. It reaches a maximum at the center of the rod and continuously drops in value until the ends of the rod are reached. The variation in permeability can be approximated by:

TABLE 48.4 Magnetic Properties of Typical Core Material

Name	Composition	Manufacturer	μ_i	μ_{max}
Mild steel	0.2 C, 99 Fe		120	2000
Silicon iron	4.0 Si, 96 Fe		500	7000
CN20	Ni-Zn Ferrite	Ceramic Magnetics	800	4500
MN60	Mn-Zn Ferrite	Ceramic Magnetics	5000	10,500
"49" Alloy	48 Ni, 52 Fe	Carpenter	6500	75,000
2605S-2	Fe-based amorphous alloy	Allied-Signal	10,000	600,000
4-79 Permalloy	4 Mn, 79 Ni, 17 Fe	Magnetics	20,000	100,000
Mumetal	5 Cu, 2 Cr, 77 Ni, 16 Fe	Magnetics	20,000	100,000
HyMu "80"	4.2 Mo, 80 Ni, 15 Fe	Carpenter	50,000	200,000
2826MB	NiFe-based amorphous alloy	Allied-Signal	100,000	800,000

Note: μ_i is the slope of the magnetization curve at the origin. μ_{max} is the maximum incremental slope of the magnetization curve.

$$\mu(l) = \mu_a \left[1 - F \left(\frac{l}{l_0} \right)^2 \right] \tag{48.23}$$

where l is the distance from the center of the rod to the measurement point, l_0 is the half length of the rod, and F is a constant that varies from 0.72 to 0.96. The average permeability seen by the coil is the integral of Equation 48.23 over the length of the coil:

$$\bar{\mu} = \mu_a \left[1 - F \left(\frac{l_w}{l_c} \right)^2 \right] \tag{48.24}$$

where l_w is the length of the winding and l_c is the length of the core. Equation 48.24 is substituted into Equation 48.19 to compute the rod's effective relative permeability which is used in Equation 48.13 to compute sensitivity.

The inductance of the rod antenna can be computed using the following equations:

$$L = \frac{\mu_0 \mu_e n^2 \pi (d+t)^2 l_w}{4 l_c} \tag{48.25}$$

$$\mu_e = 1 + \left(\frac{d_c}{d+t} \right)^2 \left[\mu_a f(l_w/l_c) - 1 \right] \tag{48.26}$$

$$f(l_w/l_c) = 1.9088 - 0.8672(l_w/l_c) - 1.1217(l_w/l_c)^2 + 0.8263(l_w/l_c)^3 \tag{48.27}$$

The function $f(l_w/l_c)$ accounts for the variation in flux density from the middle of the winding to its ends and assumes the winding is centered about the middle of the core.

Equations 48.15 and 48.16 can be used to compute the resistance and capacitance of a rod antenna.

Signal Conditioning

To be useful, the induction coil signal must be conditioned using either a voltage or a current amplifier. Figure 48.6 illustrates the circuit configurations for both of these signal conditioning methods. The voltage

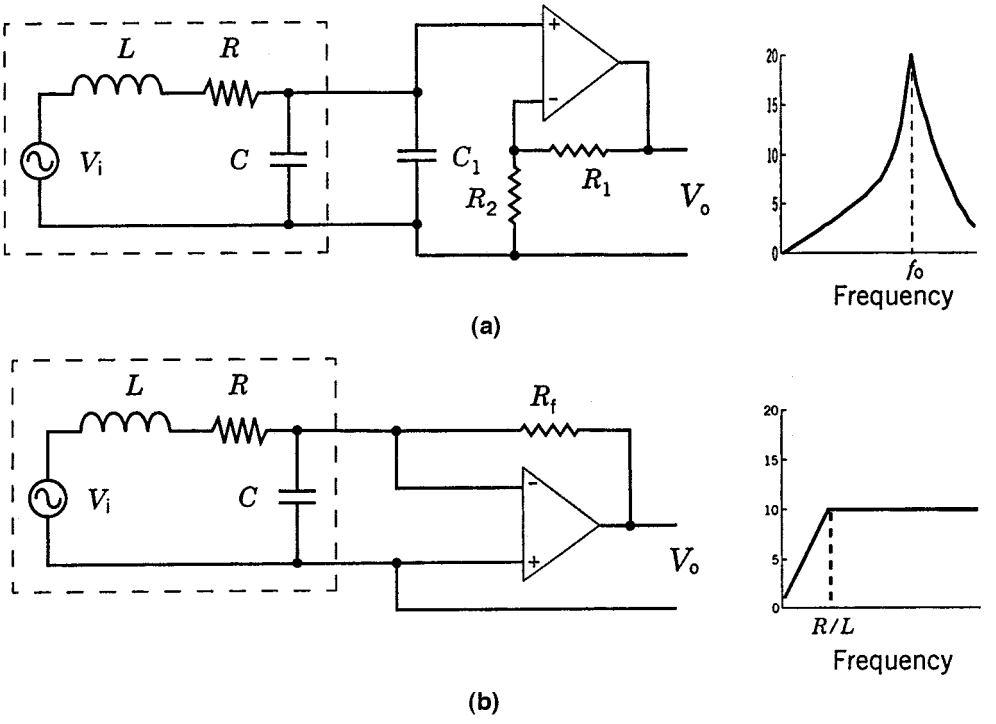

FIGURE 48.6 (a) The amplitude of a voltage-amplified induction coil signal is proportional to the frequency and strength of the field. (b) The amplitude of a current-amplified induction coil signal is only proportional to field strength beyond its L/R corner frequency.

amplifier can have either a single-ended or differential input and it can be tuned or untuned. The signal output of the voltage amplifier is proportional to the magnitude and frequency of the field for frequencies well below resonance. Its output will peak at the resonant frequency of the coil or at the tuning frequency. Because its output signal depends on both the frequency and strength of the magnetic field, the voltage amplifier is more suited to narrow band or tuned frequency applications.

In the current amplifier configuration, the induction coil terminals are connected to a virtual ground. As long as the product of the amplifier forward gain and the coil ohmic resistance is much greater than the feedback resistor, the output signal magnitude is independent of the frequency of the magnetic field beyond the R/L (rad s^{-1}) corner of the coil. This remains true up to the coil's resonant frequency. For this reason, the current amplifier configuration is particularly suited to broadband magnetic field strength measurements. The current amplifier configuration minimizes intermodulation distortion in induction coils with magnetic cores. The current flowing through the coil produces a magnetic field that opposes the ambient field. This keeps the net field in the core near zero and in a linear region of the B–H curve.

Current-amplifier-based induction coil magnetometers have been built that have a flat frequency response from 10 Hz to over 200 kHz. Some magnetometers designed for geophysical exploration applications have low frequency corners that extend down to 0.1 Hz. For further information on this subject, see [8, 9].

The Fluxgate Magnetometer

The fluxgate magnetometer has been and is the workhorse of magnetic field strength instruments both on Earth and in space. It is rugged, reliable, physically small, and requires very little power to operate. These characteristics, along with its ability to measure the vector components of magnetic fields over a

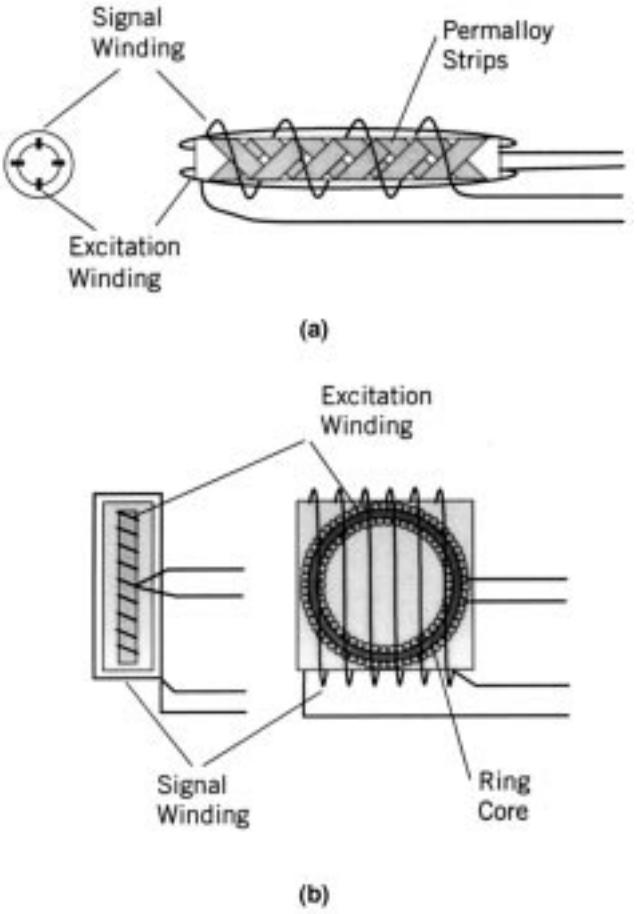

FIGURE 48.7 In Schonstedt (a) and ring core (b) fluxgate sensors, the excitation field is at right angles to the signal winding axis. This configuration minimizes coupling between the excitation field and the signal winding.

0.1 nT to 1 mT range from dc to several kHz, make it a very versatile instrument. Geologists use them for exploration and geophysicists use them to study the geomagnetic field (about 20 μT to 75 μT on the Earth's surface). Satellite engineers use them to determine and control the attitude of spacecraft, scientists use them in their research, and the military uses them in many applications, including mine detection, vehicle detection, and target recognition. Some airport security systems use them to detect weapons.

The Fluxgate

The heart of the magnetometer is the *fluxgate*. It is the transducer that converts a magnetic field into an electric voltage. There are many different fluxgate configurations. Two of the more popular ones are shown in Figure 48.7. A very comprehensive explanation of the fluxgate principle and the different fluxgate configurations is given in [10].

The ring core fluxgate is constructed from a thin ribbon of easily saturable ferromagnetic material, such as 4-79 Permalloy wrapped around a bobbin to form a ring or toroid. As shown in Figure 48.8, an alternating current is applied through a coil that is wound about the toroid. This creates a magnetic field that circulates around the magnetic core. This magnetic field causes the flux in the ferrous material to periodically saturate first clockwise and then counterclockwise. A pick-up (signal) winding is wrapped around the outside of the toroid. While the ferrous material is between saturation extremes, it maintains an average permeability much greater than that of air. When the core is in saturation, the core permeability

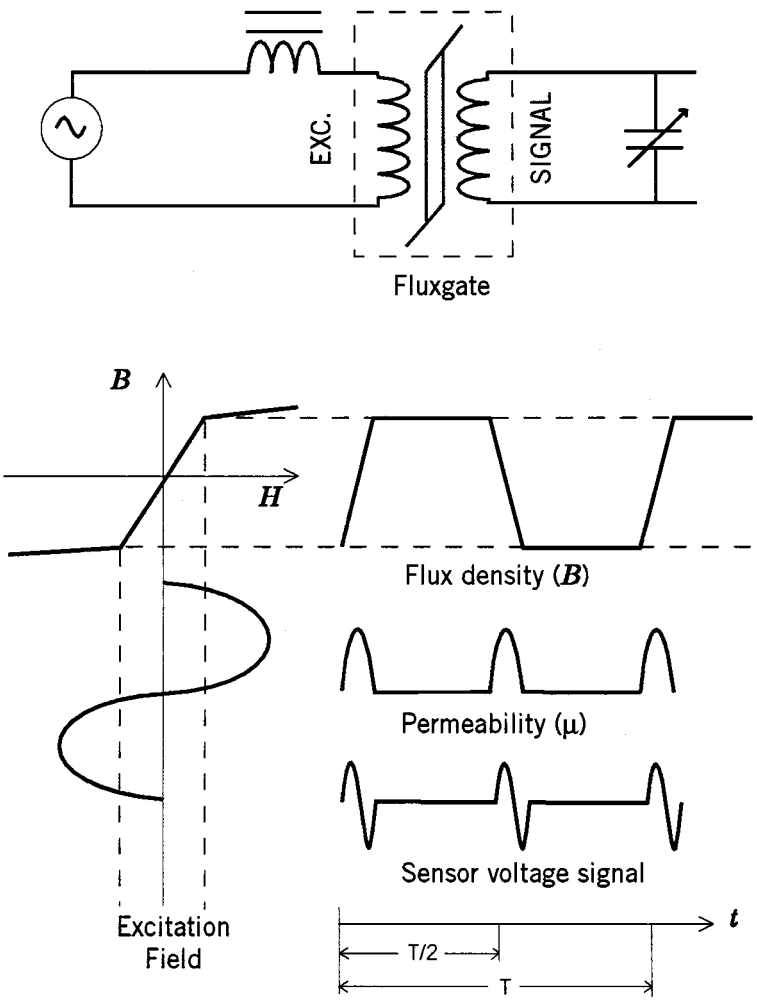

FIGURE 48.8 The excitation field of a fluxgate magnetometer alternately drives the core into positive or negative saturation, causing the core's effective permeability to switch between 1 and a large value twice each cycle.

becomes equal to that of air. If there is no component of magnetic field along the axis of the signal winding, the flux change seen by the winding is zero. If, on the other hand, a field component is present along the signal winding axis, then each time the ferrous material goes from one saturation extreme to the other, the flux within the core will change from a low level to a high level. According to Faraday's law, a changing flux will produce a voltage at the terminals of the signal winding that is proportional to the rate of change of flux. For dc and low-frequency magnetic fields, the signal winding voltage is:

$$e(t) = nA\frac{d(\mu_0\mu_e H)}{dt} = nA\mu_0 H\frac{d\mu_e(t)}{dt} \tag{48.28}$$

where H = Component of the magnetic field being measured
n = Number of turns on the signal winding
A = Cross-sectional area of the signal winding
$\mu_e(t)$ = Effective relative permeability of the core

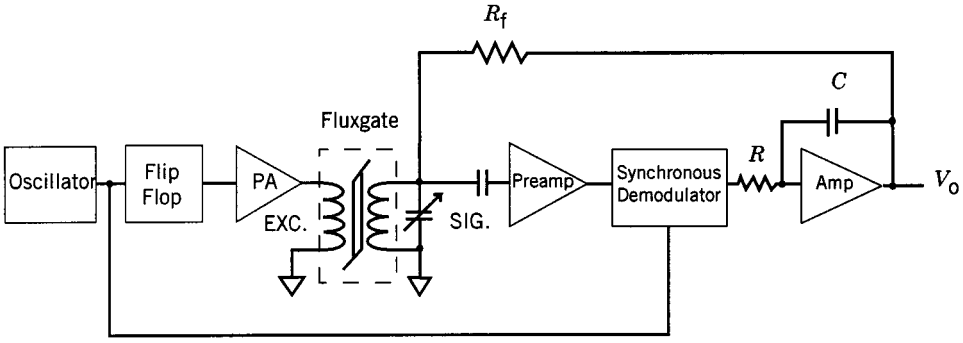

FIGURE 48.9 Typical circuit configuration for a field feedback fluxgate magnetometer. The sensor output is ac amplified, synchronously demodulated, and filtered. A magnetic field that nulls the ambient field at the sensor is produced by connecting the resistor R_f between the output and the signal winding.

As the core permeability alternates from a low value to a high value, it produces a voltage pulse at the signal winding output that has an amplitude proportional to the magnitude of the external magnetic field and a phase indicating the direction of the field. The frequency of the signal is twice the excitation frequency since the saturation-to-saturation transition occurs twice each excitation period.

The discussion about effective permeability in the induction coil section applies here as well. Consult [10, 13] for comprehensive discussions about fluxgate effective permeability and signal characteristics as they relate to excitation field level, excitation waveform, and winding geometry.

Signal Conditioning

The signal from the fluxgate is an amplitude-modulated suppressed carrier signal that is synchronous with the second harmonic of the excitation signal. In a simple low-power magnetometer, this signal is converted to the base band using a synchronous demodulator, filtered, and presented as the final output. Example circuits are given in [11, 12]. The accuracy of magnetometers that use this open-loop architecture is limited by the linearity of the core's magnetization curve and is about 5% for Earth's field (60 μT) applications.

More precise and stable magnetometers use magnetic field feedback rather than the open-loop structure described above. A simplified schematic of a typical second harmonic field feedback fluxgate magnetometer is shown in Figure 48.9. The circuitry to the left of the fluxgate is called the excitation circuit. It consists of an oscillator tuned to twice the excitation frequency, a flip-flop that divides the oscillator frequency by two, and a power amplifier driven by the flip-flop and, in turn, provides the excitation current to the excitation winding.

The circuitry to the right of the fluxgate is called the signal channel circuit. It amplifies the output from the fluxgate signal winding, synchronously demodulates the ac signal using the oscillator signal as a reference, integrates and amplifies the base band output, and then feeds back the output through a resistor to the signal winding. The fed-back signal produces a magnetic field inside the sensor that opposes the external field. This keeps the field inside the sensor near zero and in a linear portion of the magnetization curve of the ferromagnetic core.

The flow diagram for the magnetometer is given in Figure 48.10. The external field H_a is opposed by the feedback field H_f, and the difference is converted into a voltage signal (K_s represents the transfer function from field to voltage). This signal is amplified (A), and the amplified signal is converted into a current I_f and then into the feedback field (K_c represents the transfer function from current to field). The overall transfer function for the magnetometer is:

$$\frac{V_0}{H_a} = \frac{AK_s}{1 + \dfrac{K_c AK_s}{R_f}} \tag{48.29}$$

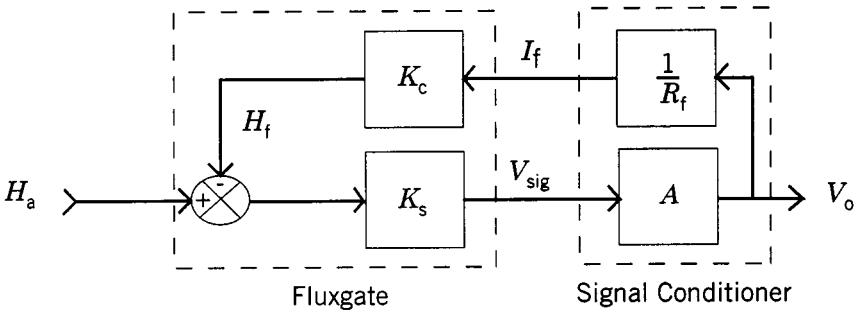

FIGURE 48.10 Block diagram of a field feedback fluxgate magnetometer. K_c is the current-to-field constant for the coil. K_s is the field-to-voltage transduction constant for the sensor. The feedback field H_f opposes the ambient field H_a, thus keeping the net sensor field very small.

The amplifier gain is normally very high such that the second term in the denominator is much larger than one, and Equation 48.29 reduces to

$$\frac{V_0}{H_a} = \frac{R_f}{K_c} \tag{48.30}$$

Under these circumstances, the transfer function becomes almost completely determined by the ratio of R_f (the feedback resistor) to K_c (the current-to-field coil constant of the sensor winding). Both of these constants can be very well controlled. The consequence of this circuit topology is a highly stable and accurate magnetometer that is insensitive to circuit component variations with temperature or time. An accuracy of 1% over a temperature range of –80°C to 80°C is easily achievable. Accuracy and stability can be improved using a current feedback circuit, like the one described in [13], that compensates for the resistance of the signal winding or by using a separate feedback winding and a high-quality voltage-to-current converter instead of a simple feedback resistor.

The SQUID Magnetometer

Brian D. Josephson in 1962, while a graduate student at Cambridge University, predicted that superconducting current could flow between two superconductors that are separated by a thin insulation layer. The magnitude of the superconductor (critical) current through this "Josephson junction" is affected by the presence of a magnetic field and forms the basis for the SQUID magnetometer.

Figure 48.11 illustrates the general structure of a Josephson junction and the voltage–current (V–I) relationship. Two superconductors (e.g., niobium) are separated by a very thin insulating layer (e.g., aluminum oxide). The thickness of this layer is typically 1 nm. When the temperature of the junction is reduced to below 4.2 K (–269°C), a superconductor current will flow in the junction with 0 V across the junction. The magnitude of this current, called the critical current I_c, is a periodic function of the magnetic flux present in the junction. Its maximum magnitude occurs for flux values equal to $n\phi_0$, where ϕ_0 is one flux quantum (2 fW), and its minimum magnitude occurs for flux values equal to $(n + ½)\phi_0$. The period is one flux quantum. This phenomenon is called the "dc Josephson effect" and is only one of the "Josephson effects."

Magnetometers based on the Superconducting Quantum Interference Device (SQUID) are currently the most sensitive instruments available for measuring magnetic field strength. SQUID magnetometers measure the change in the magnetic field from some arbitrary field level; they do not intrinsically measure the absolute value of the field. Biomedical research is one of the more important applications of SQUID magnetometers. SQUID magnetometers and gradiometers (measure spatial variation in the magnetic field) have the high sensitivities needed to measure the weak magnetic fields generated by the body [15].

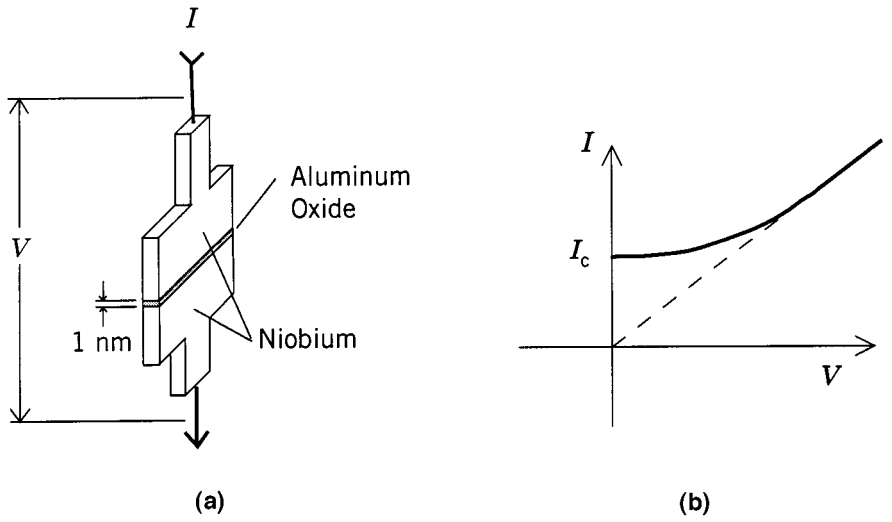

FIGURE 48.11 The Josephson junction in (a) consists of a superconductor such as niobium separated by a thin insulation layer. The voltage (V) vs. current (I) curve in (b) shows that a superconducting current flows through the junction with zero volts across the junction.

Other application areas include paleomagnetics (measuring remnant magnetism in rocks) and magnetotellurics (Earth resistivity measurements). Descriptions of these applications as well as the general theory of SQUIDs can be found in [16]. Clark [17], one of the pioneers in SQUID magnetometers, provides a good contemporary overview of SQUID technology and applications.

A dc SQUID magnetometer uses two Josephson junctions in the two legs of a toroid as shown in Figure 48.12(a). The toroid is biased with a constant current that exceeds the maximum critical current of the junctions. When the flux through the toroid is an integral multiple of ϕ_0, the voltage across the junctions is determined by the intersection of I_b and the $n\phi_0$ V–I curve (point A). As the flux increases, the critical current decreases. The V–I curve and thus the intersection point move to the right (the junction voltage increases). The critical current reaches a minimum when the flux has increased by $\frac{1}{2}\phi_0$ and the junction voltage is at its maximum (point B). As the flux continues to increase, the critical current increases back toward its maximum value and the junction voltage decreases. Thus, the period of the flux cycle is ϕ_0.

Signal Conditioning

Figure 48.13 is a block diagram of one implementation of a dc SQUID magnetometer that can be used for wide dynamic range field measurements. A large superconducting loop, which is exposed to the magnetic field being measured, is connected to a multiturn signal winding that is magnetically coupled directly to the SQUID. At cryogenic temperatures, the loop and signal winding effectively form a dc induction coil. External flux applied to the coil will generate a current in the loop that keeps the net flux within the loop constant, even for dc magnetic fields. The signal winding magnifies the flux that is applied to the SQUID.

The SQUID is magnetically biased at an optimal sensitivity point. A small ac magnetic field at 100 kHz to 500 kHz is superimposed on the bias field. The output of the SQUID is a suppressed carrier amplitude modulated signal where the amplitude indicates the change in magnetic field from the bias point, and the phase indicates the polarity of the change. The output signal is amplified and then synchronously demodulated down to the base band. The resulting dc signal is amplified and fed back through a resistor to a coil coupled to the SQUID. The current through the coil generates a magnetic field at the SQUID that opposes the applied field. This keeps the SQUID operating point very near the bias point. The scale

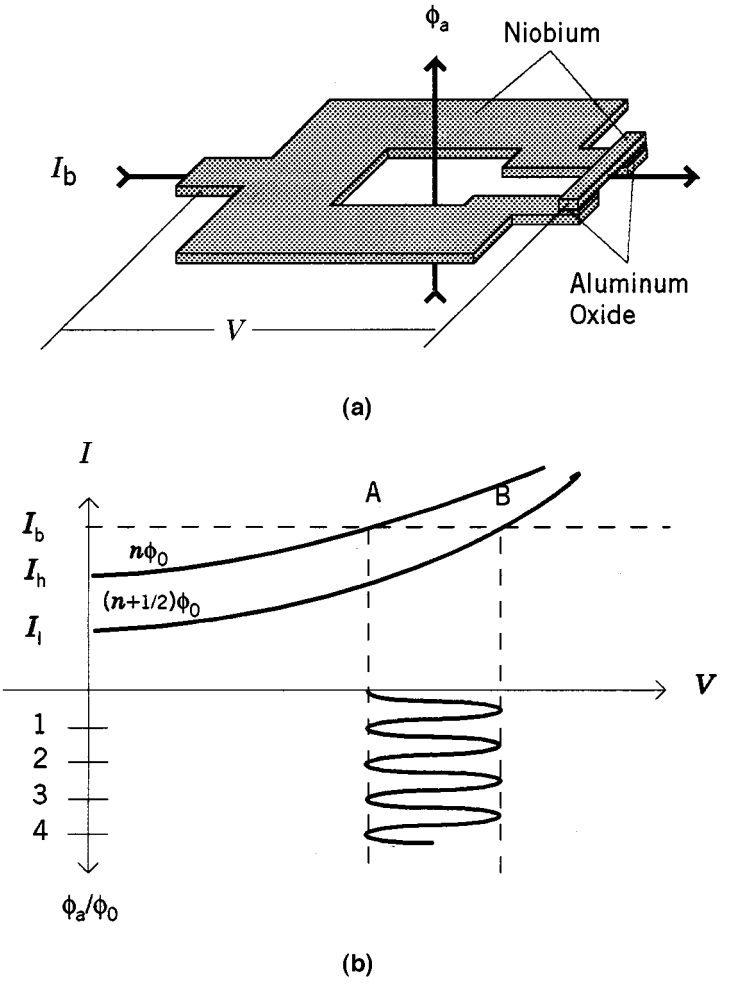

FIGURE 48.12 Use of a dc SQUID to measure magnetic flux. The dc SQUID in (a) consists of a superconductor loop and two Josephson junctions with a bias current that is greater than the maximum critical current I_h. The *V–I* curve in (b) illustrates how the voltage across the SQUID oscillates with a period equal to one flux quantum ϕ_0.

factor of the magnetometer depends on the feedback resistor and the coil constant of the feedback winding in the same manner that it does for a field feedback fluxgate magnetometer.

The pick-up loop, signal coil, SQUID, feedback coil and feedback resistor are kept in a cryogenic temperature chamber and, except for the pick-up coil, are magnetically shielded. The rest of the circuit is operated at room temperature.

48.3 High-Field Vector Gaussmeters

The Hall Effect Gaussmeter

The Hall effect device, which is probably the most familiar and widely used sensor for measuring strong magnetic fields, is based on the discovery of the Hall effect by Edwin H. Hall in 1897. The Hall effect is a consequence of the Lorentz force law, which states that a moving charge *q*, when acted upon by a magnetic induction field $\vec{B}$, will experience a force $\vec{F}$ that is at right angles to the field vector and the velocity vector *v* of the charge as expressed by the following equation:

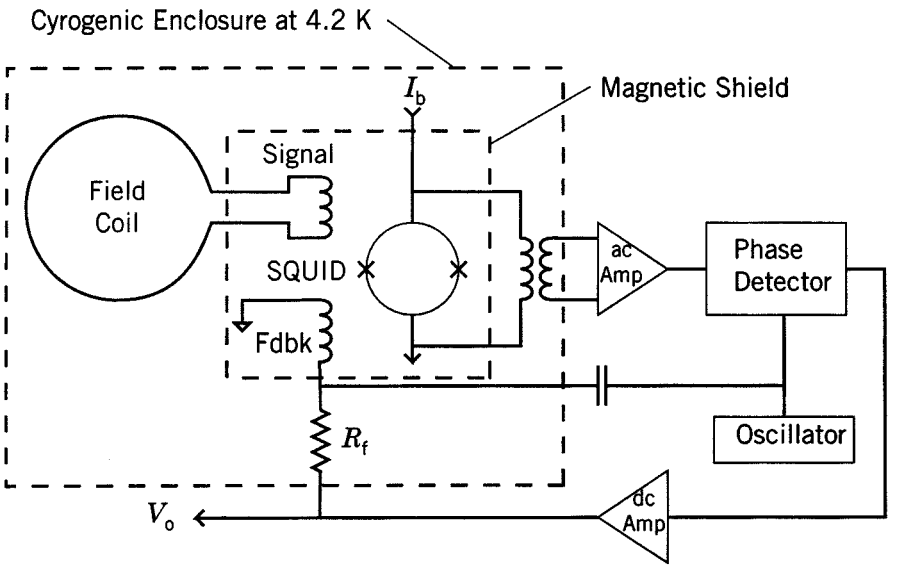

FIGURE 48.13 Wide dynamic range dc SQUID magnetometer. A magnetic field produced by connecting resistor R_f between the output and a feedback coil keeps the field in the SQUID within one flux quantum over its operating range. (Adapted from Wellstood, Heiden and Clark, 1984.)

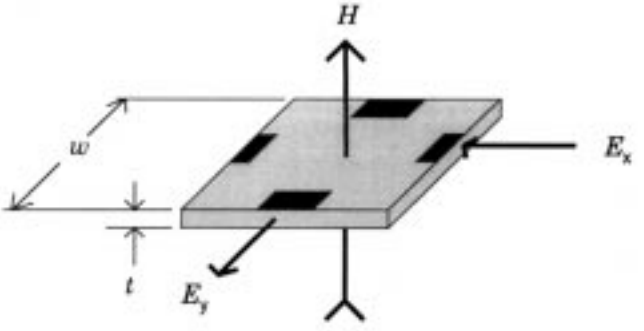

FIGURE 48.14 Hall effect sensor. A magnetic field H applied normal to the surface of the sensor, which is conducting current along the x-direction, will generate a voltage along the y-direction. E_x is the applied electric field along the x-direction, and E_y is the Hall effect electric field along the y-direction.

$$\vec{F} = -q\left(\vec{E} + \vec{v} \times \vec{B}\right) \tag{48.31}$$

The Hall effect device consists of a flat, thin rectangular conductor or semiconductor with two pairs of electrodes at right angles to one another as illustrated in Figure 48.14. An electric field E_x is applied along the x or control axis. When a magnetic field B_z is applied perpendicular to the surface of the device, the free charge, which is flowing along the x-axis as a result of E_x, will be deflected toward the y or Hall voltage axis. Since current cannot flow in the y-axis under open-loop conditions, this will cause a buildup of charge along the y-axis that will create an electric field which produces a force opposing the motion of the charge:

$$E_y = v_x B_z \tag{48.32}$$

where v_x is the average drift velocity of the electrons (or majority carriers). In a conductor that contains n free charges per unit volume having an average drift velocity of v_x, the current density is:

$$J_x = qnv_x \tag{48.33}$$

and

$$E_y = \frac{J_x B_z}{qn} = R_H J_x B_z \tag{48.34}$$

where R_H is called the Hall coefficient.

A semiconductor is treated in terms of the mobility μ (drift velocity/field) of the majority carrier (electron or hole) and conductivity σ. In this case,

$$E_y = \mu E_x B_z \text{ and } E_x = \frac{J_x}{\sigma} \tag{48.35}$$

Therefore,

$$E_y = \frac{\mu}{\sigma} J_x B_z \text{ and } R_H = \frac{\mu}{\sigma} \tag{48.36}$$

The value of R_H varies substantially from one material to another and is both temperature and field magnitude dependent. Its characteristics can be controlled to a certain extent by doping the base material with some impurities. For example, doping germanium with arsenic can reduce the temperature dependence at the expense of magnitude.

The voltage measured across the *y*-axis terminals is the integral of the electric field along the *y*-axis. If a constant control current I is flowing along the x axis, then:

$$J_x = \frac{I}{wt} \tag{48.37}$$

and the measured output voltage is:

$$e_y = \frac{R_H I B_z}{t} \tag{48.38}$$

where t is thickness (m) and w is the distance between the *y*-axis terminals.

Another characteristic specified by manufacturers of Hall effect devices is the magnetic sensitivity γ_b at the rated control current I_c:

$$\gamma_b = \frac{e_y}{B_z} = \frac{R_H I_c}{t} \tag{48.39}$$

Although conductors such as copper (Cu) can be used to make a Hall effect device, semiconductor materials, such as gallium arsenide (GaAs), indium antimonide (InSb), and indium arsenide (InAs), produce the highest and most stable Hall coefficients. InAs, because of its combined low temperature coefficient of sensitivity (<0.1%/°C), low resistance, and relatively good sensitivity, is the material favored by commercial manufacturers of Hall effect devices.

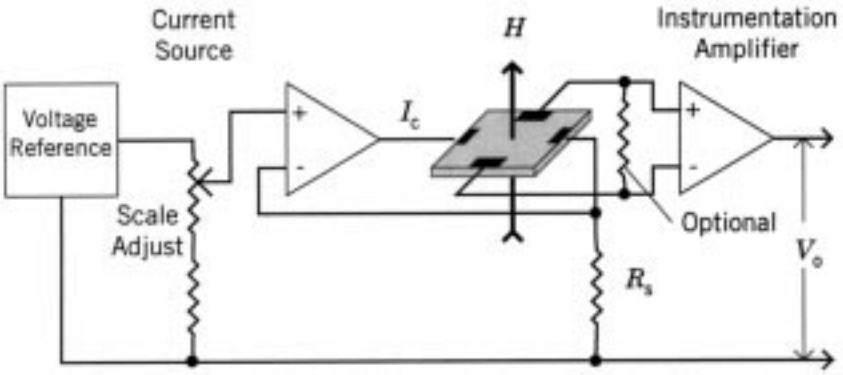

FIGURE 48.15 Example of how to construct a Hall effect gaussmeter. The operational amplifier and resistor R_s form a stable constant-current source for the Hall effect sensor. An instrumentation or differential amplifier amplifies and scales the Hall voltage. A load resistor is sometimes required across the Hall voltage output terminals.

The typical control current for Hall effect devices is 100 mA, but some do operate at currents as low as 1 mA. Sensitivities range from 10 mV/T to 1.4 V/T. Linearity ranges from ¼% to 2% over their rated operating field range. The control input and the voltage output resistance are typically in the range of 1 Ω to 3 Ω. The sensor element is usually tiny (on the order of 10 mm square by 0.5 mm thick), and a three-axis version can be housed in a very small package. These devices are most effective for measuring flux densities ranging from 50 μT to 30 T.

Signal Conditioning

A simple Hall effect gaussmeter can be constructed using the signal conditioning circuit shown in Figure 48.15. The voltage reference, operational amplifier, and sense resistor R_s form a precision constant-current source for the Hall effect device control current I_c. For best performance, the voltage reference and R_s should be very stable with temperature and time. A general-purpose operational amplifier can be used for low control currents. A power amplifier is required for control currents above 20 mA.

The Hall voltage can be conditioned and amplified by any high input impedance (>1 kΩ) differential amplifier. A precision instrumentation amplifier is a good choice because it has adequate input impedance, its gain can be determined by a stable resistor, and the amplifier zero offset trim resistor can be used to cancel the zero offset of the Hall effect device. Some devices require a load resistor across the Hall voltage terminal to achieve optimum linearity.

The zero offset and $1/f$ noise of the Hall voltage amplifier limit the performance of a Hall effect gaussmeter for low field strength measurements. Sometimes, these effects can be reduced by using an ac precision current source. The ac amplitude modulated Hall voltage can then be amplified in a more favorable frequency band and synchronously detected to extract the Hall voltage signal. If the field to be measured requires this amount of signal conditioning, it probably is better to use a fluxgate magnetometer for the application.

The Magnetoresistive Gaussmeter

The magnetoresistance effect was first reported by William Thomson (Lord Kelvin) in the middle of the 19th century. He found that a magnetic field applied to a ferromagnetic material caused its resistivity to change. The amount of change depends on the magnetization magnitude and the direction in which the current used to measure resistivity is flowing. Nickel–iron alloys show the greatest change in resistivity (about 5% maximum). Figure 48.16 illustrates how the resistivity changes in Permalloy (a nickel–iron alloy) for a field applied parallel to the current flow. As magnetic field is increased, the change in resistivity increases and asymptotically approaches its maximum value when the material approaches saturation. Bozorth [6] points out that the shape of the curve and the magnitude of the change depend on the

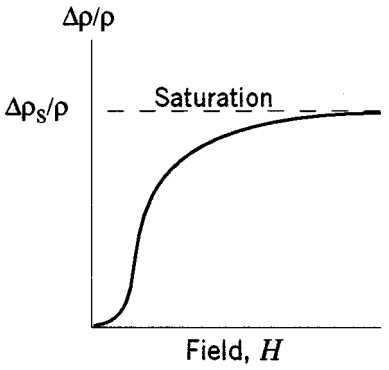

FIGURE 48.16 Change in resistivity in a ferromagnetic material. As field is applied, the resistivity changes rapidly at first. As the material approaches magnetic flux saturation, the resistivity change approaches its maximum value.

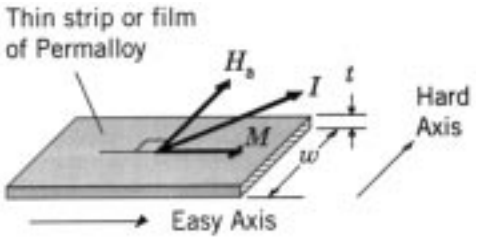

FIGURE 48.17 An AMR resistor element. During fabrication, a magnetic field is applied along the strip's length to magnetize it and establish its easy axis. Current I is passed through the film at 45° to the easy or anisotropic axis. A magnetic field H_a applied at right angles to the magnetization vector M causes the magnetization vector to rotate and the magnetoresistance to change.

composition of the alloy. Permalloy with 80% Ni and 20% Fe provides a high magnetoresistance effect with near-zero magnetostriction and is a favorite material for magnetoresistors.

The change in resistivity in permalloy film [18] is also a function of the angle θ between the magnetization direction and the current direction:

$$\rho(\theta) = \rho_0 + \Delta\rho_m \cos^2\theta \tag{48.40}$$

where $\Delta\rho_m$ is the magnetoresistivity anisotropy change and ρ_0 is the resistivity for $\theta = \pi/2$.

It was mentioned earlier that magnetic materials have anisotropic magnetic properties (their magnetic properties are direction dependent). The physical shape of an object (see the discussion on demagnetizing factor above) and the conditions that exist during fabrication strongly determine its anisotropic characteristics. A thin long film of permalloy can be made to have highly uniaxial anisotropic properties if it is exposed to a magnetizing field during deposition. This characteristic is exploited in the anisotropic magnetoresistance (AMR) sensor.

The basic resistor element in an AMR is a thin rectangular shaped film as shown in Figure 48.17. One axis, called the anisotropy or easy axis, has a much higher susceptibility to magnetization than the other two. The easy axis is normally along the length of the film. Because of its thinness, the axis normal to the film has virtually no magnetic susceptibility. The axis transverse to the easy axis (across the width) has very little susceptibility as well.

A bias field H_b is used to saturate the magnetization along the easy axis and establish the magnetization direction for zero external field. For a simplified analysis, the film can be modeled as a single domain.

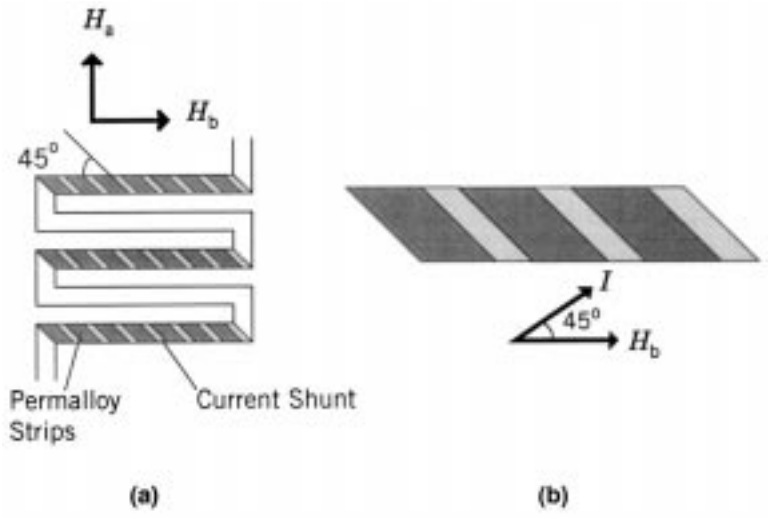

FIGURE 48.18 Magnetoresistor construction. (a) A typical AMR element consists of multiple strips of permalloy connected together in a serpentine pattern. Current shunts force the current to flow through the permalloy at 45° to the easy axis. (b) A close-up view.

The effect of an external field in the plane of the film and normal to the anisotropy axis is to rotate the magnetization vector and, according to Equation 48.40, change the resistivity. Kwiatkowski and Tumanski [19] stated that the change in resistance of the film can be approximated by Equation 48.41:

$$\Delta R \approx R_s \frac{\Delta\rho_m}{\rho}\left(h_a^2 \cos 2\theta + h_a \sqrt{1-h_a^2}\sin 2\theta - \frac{1}{2}\cos 2\theta\right) \tag{48.41}$$

where h_a is the normalized externally applied field (i.e., $h_a = H_a/H_k$), R_s is the nominal resistance, and $\Delta\rho_m/\rho$ is the maximum resistivity change. H_k is the anisotropy field. Optimum linear performance is obtained when $\theta = \pi/4$ and Equation 48.41 reduces to:

$$\Delta R \approx R_s \frac{\Delta\rho_m}{\rho}\frac{1}{H_k + H_b} H_a \tag{48.42}$$

The anisotropy field is given by:

$$H_k = \sqrt{H_{k0}^2 + \left(NM_s\right)^2} \tag{48.43}$$

where H_{k0} is the film anisotropy field, N is the demagnetizing factor (≈ thickness(t)/width(w)) and M_s is the saturation magnetization.

An AMR is constructed using long thin film segments of deposited permalloy. During deposition, a magnetic field is applied along the length of the film to establish its easy axis of magnetization. The shape of the film also favors the length as an easy axis. As shown in Figure 48.18, a series of these permalloy films is connected together to form the magnetoresistor. The current is forced to flow at a 45° angle to the easy axis by depositing thin strips of highly conductive material (e.g., gold) across the permalloy film. The level of magnetization of the film is controlled by a bias field that is created through the deposition of a thin layer of cobalt over the resistors, which is then magnetized parallel to the easy axis of the permalloy.

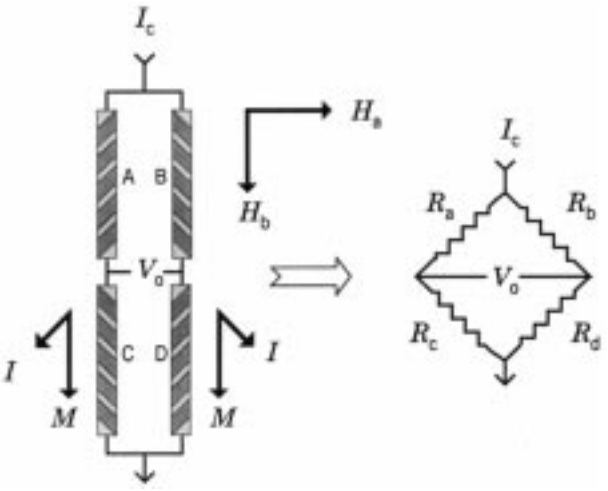

FIGURE 48.19 AMR bridge sensor. In an AMR bridge, the current shunts of resistors A and D are the same and reversed from B and C. Thus, the resistors on diagonal legs of the bridge have the same response to an applied field and opposite that of the other diagonal pair. Bridge leg resistance varies from 1 kΩ to 100 kΩ.

A typical AMR sensor suitable for a gaussmeter or magnetometer consists of four AMRs connected in a Wheatstone bridge as shown in Figure 48.19. The transfer function polarity of the A and D resistors is made to be opposite that of the B and C resistors by rotating the current shunt 90°. This complimentary arrangement enhances the output voltage signal for a given field by a factor of four over a single resistor. Kwiatkowski and Tumanski [19] showed that the transfer function for the bridge configuration is described by:

$$v = IR_s \frac{\Delta\rho_m}{\rho} \cos 2\Delta\varepsilon h_a \sqrt{1-h_a^2} \tag{48.44}$$

Where:

$$\cos 2\Delta\varepsilon = \frac{H_{k0}^2 + H_k^2 - \left(NM_s\right)^2}{2H_{k0}H_k} \tag{48.45}$$

$$h_a = \frac{H_a}{H_k + H_b} \tag{48.46}$$

For best linearity, $H_a < 0.1\ H_k$. The linearity of the bridge can be controlled during fabrication by adjusting the l/w ratio and H_{k0}. The bias field can also be used to optimize linearity and establish the measurement field range. Some transfer functions for a typical AMR bridge [20] are shown in Figure 48.20. A more comprehensive discussion of AMR theory can be found in [21–23].

Signal Conditioning

Conventional Wheatstone bridge signal conditioning circuits can be used to process the AMR bridge. The bridge sensitivity and zero offset are proportional to the bridge voltage, so it is important to use a well-regulated supply with low noise and good temperature stability.

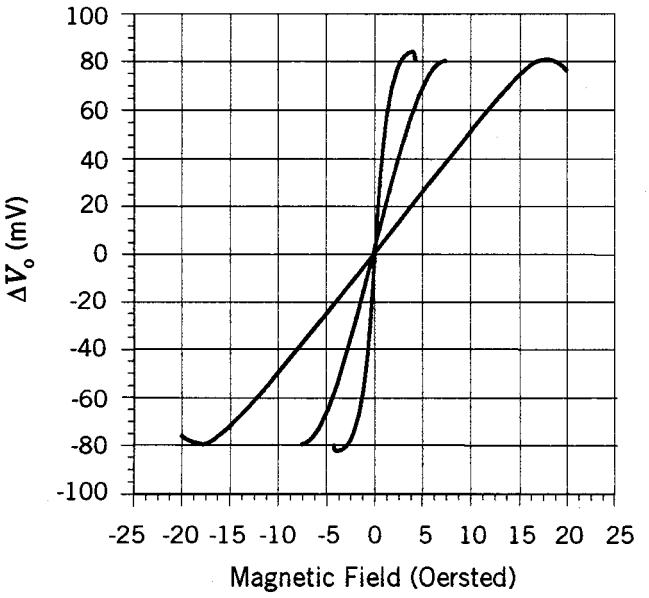

FIGURE 48.20 Typical AMR bridge sensor transfer functions. The sensitivity of an AMR bridge can be adjusted by changing its bias field. Increases in sensitivity are accompanied by corresponding decreases in range.

As Equation 48.44 shows, the polarity of the transfer function is determined by the polarity of (H_k + H_b). If the sensor is exposed to an external field that is strong enough to reverse this field, then the transfer function polarity will reverse. To overcome this ambiguity, the polarity should be established prior to making a measurement. This can be accomplished by momentarily applying a strong magnetic field along the easy axis of the AMR bridge. Some commercial AMR bridges come with a built-in method for performing this action.

Figure 48.21 is a block diagram for a signal conditioner that takes advantage of the bias field polarity flipping property to eliminate zero offset errors and low frequency 1/*f* noise. A square wave oscillator is used to alternately change the direction of the bias field and thus the polarity of the transfer function. The duration of the current used to set the bias field direction should be short in order to minimize power consumption. The amplitude of the ac signal from the bridge is proportional to the field magnitude, and its phase relative to the oscillator gives the field direction. This signal can be amplified and then phase-detected to extract the field-related voltage. Optionally, the output signal can be fed back through a coil that produces a magnetic field opposing the field being measured. This feedback arrangement makes the AMR bridge a null detector and minimizes the influence of changes in its transfer function on overall performance. Of course, the added circuitry increases the size, cost, and complexity of the instrument.

48.4 Scalar Magnetometers

Scalar magnetometers measure the magnitude of the magnetic field vector by exploiting the atomic and nuclear properties of matter. The two most widely used scalar magnetometers are the proton precession and the optically pumped magnetometer. When operated under the right conditions, these instruments have extremely high resolution and accuracy and are relatively insensitive to orientation. They both have several common operating limitations. The instruments require the magnetic field to be uniform throughout the sensing element volume. They have a limited magnetic field magnitude measurement range: typically 20 μT to 100 μT. And they have limitations with respect to the orientation of the magnetic field vector relative to the sensor element.

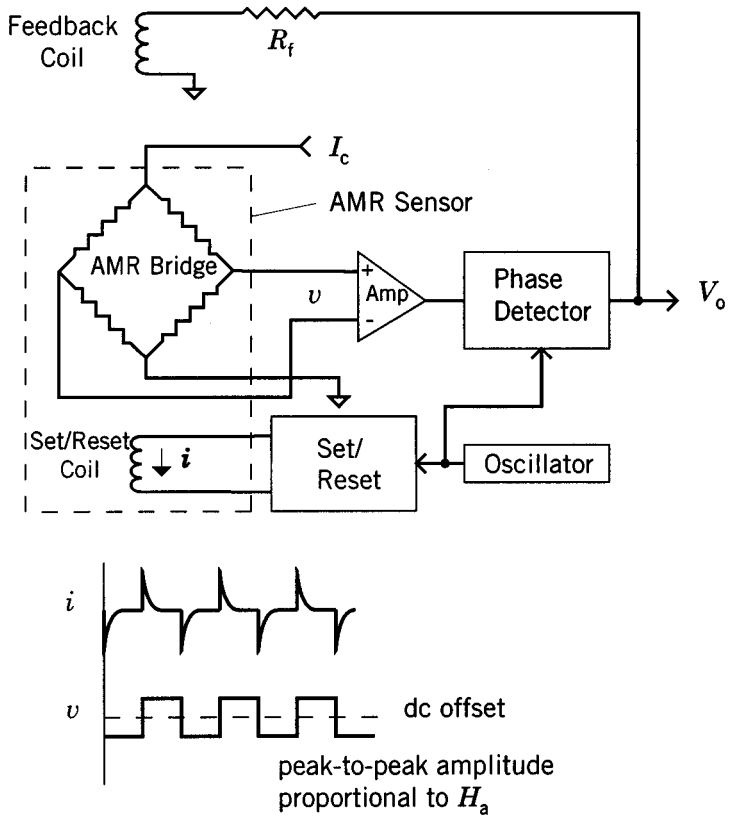

FIGURE 48.21 Example AMR gaussmeter. The magnetization direction can be alternately flipped to eliminate zero offset. The resulting ac signal can then be amplified and synchronously phase-detected to recover the field-related signal. Optionally, the range and stability of the AMR gaussmeter can be increased by connecting the output voltage through a resistor to a feedback coil that produces a field that nulls the applied field.

The proton precession magnetometer uses a strong magnetic field to polarize the protons in a hydrocarbon and then detects the precession frequency of the protons while they decay to the nonpolarized state after the polarizing field is turned off. The precession frequency is proportional to the magnitude of any ambient magnetic field that is present after the polarizing field is removed. This sampling of the magnetic field strength through the polarize-listen sequence makes the proton precession magnetometer response very slow. Maximum rates of only a few samples per second are typical. Because of its dependence on atomic constants, the proton precession magnetometer is the primary standard for calibrating systems used to generate magnetic fields and calibrate magnetometers.

The optically pumped magnetometer is based on the Zeeman effect. Zeeman discovered that applying a field to atoms, which are emitting or absorbing light, will cause the spectral lines of the atoms to split into a set of new spectral lines that are much closer together than the normal lines. The energy-related frequency interval between these hyperfine lines is proportional to the magnitude of the applied field. These energy levels represent the only possible energy states that an atom can possess. The optically pumped magnetometer exploits this characteristic by optically stimulating atoms to produce an overpopulated energy state in one of the hyperfine spectral lines and then causing the energy state to depopulate using an RF magnetic field. The RF frequency required to depopulate the energy state is equal to the spectral difference of the hyperfine lines produced by a magnetic field and, therefore, is proportional to the magnetic field strength. The optically pumped magnetometer can be used to sample the magnetic

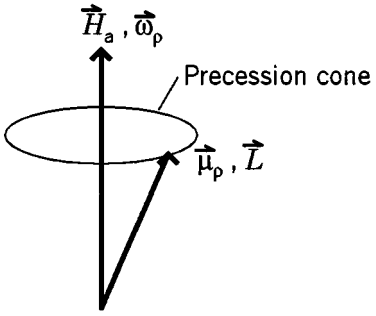

FIGURE 48.22 Nuclear precession. A spinning proton with angular momentum L and magnetic moment μ_p, when subjected to a magnetic field H_a, will precess about the field at an angular rate ω_ρ equal to $\mu_p H_a/L$.

field at a much higher rate than the proton precession magnetometer and generally can achieve a higher resolution. The sample rate and instrument resolution are interdependent.

The Proton Precession Magnetometer

The proton precession magnetometer works on the principle that a spinning nucleus, which has both angular momentum $\vec{L}$ and a magnetic moment $\vec{\mu}_p$, will precess about a magnetic field like a gyroscope, as shown in Figure 48.22. The precession frequency ω_ρ is proportional to the applied field. When the magnetic field $\vec{H}_a$ is applied to the nucleus, it will produce a torque:

$$\vec{T} = \vec{\mu}_\rho \times \vec{H}_a \tag{48.47}$$

on the nucleus. Because the nucleus has angular momentum, this torque will cause the nucleus to precess about the direction of the field. At equilibrium, the relationship between the torque, precession rate, and angular momentum is:

$$\mu_\rho \times \vec{H}_a = \vec{\omega}_\rho \times \vec{L} \tag{48.48}$$

Solving for the magnitude of the (Larmor) precession frequency, one finds that:

$$\omega_\rho = \left(\frac{\mu_\rho}{L}\right) H_a = \gamma H_a \tag{48.49}$$

where γ is called the gyromagnetic ratio and equals $(2.6751526 \pm 0.0000008) \times 10^{-8}$ T^{-1} s^{-1}.

Figure 48.23 is a block diagram of a proton precession magnetometer. The sensor is a container of hydrocarbon rich in free hydrogen nuclei. A solenoid wrapped around the container is used to both polarize the nuclei and detect the precession caused by the ambient field. Before the polarizing field is applied, the magnetic moments of the nuclei are randomly oriented, and the net magnetization is zero. Application of the polarizing field (typically 3 mT to 10 mT) causes the nuclei to precess about the field. The precession axis can be parallel or antiparallel (nuclear magnetic moment pointing in the direction of the field) to the applied field. From a quantum mechanical standpoint, the antiparallel state is a lower energy level thin the parallel sta te. In the absence of thermal agitation, which causes collisions between atoms, the fluid would remain unmagnetized. When a collision occurs, the parallel precession-axis nuclei lose energy and switch to the antiparallel state. After a short time, there are more nuclei with magnetic

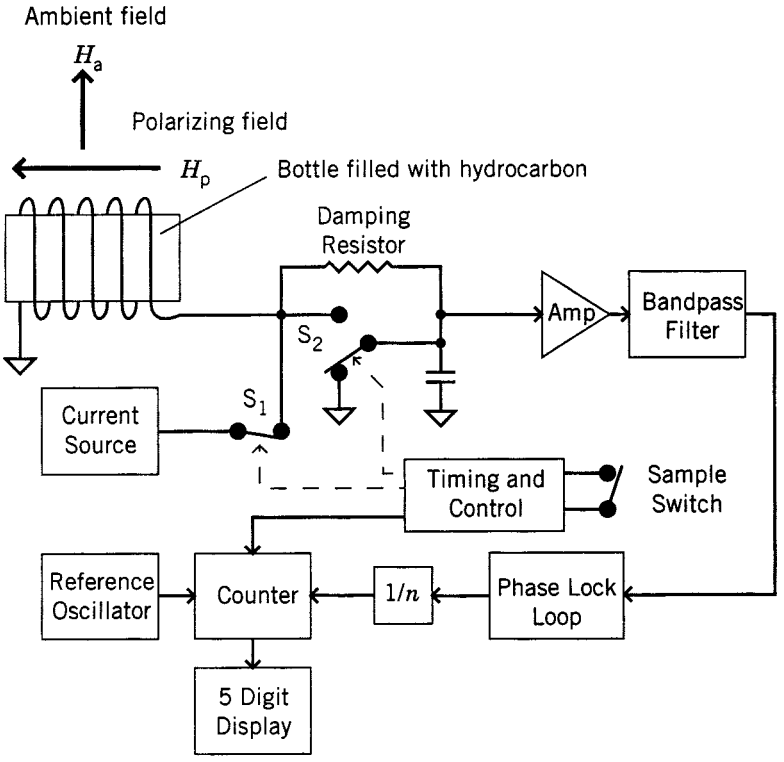

FIGURE 48.23 Typical proton precession magnetometer. A polarizing field is applied to the hydrocarbon when S1 is closed. The amplifier input is shorted to prevent switching transients from overdriving it. After a few seconds, S1 is opened and the coil is connected to the signal processor to measure the Larmor frequency.

moments pointing in the direction of the field than away from it, and the fluid reaches an equilibrium magnetization M_0. The equation that relates magnetization buildup to time is:

$$M(t) = M_0\left(1 - e^{-t/\tau_e}\right) \tag{48.50}$$

where τ_e is the spin-lattice relaxation time.

The equilibrium magnetization is based on thermodynamic considerations. From Boltzmann statistics for a system with spins of ½:

$$\frac{n_p}{n_a} = e^{2\mu_p H_a/kT} \tag{48.51}$$

where n_p is the number of precession spin axes parallel to H_a, n_a is the number of precession spin axes antiparallel to H_a, k is Boltzmann's constant, and T is temperature (kelvin). If n is the number of magnetic moments per unit volume, then:

$$n = n_p + n_a = n_a\left(1 + e^{2\mu_p H_a/kT}\right) \tag{48.52}$$

and

$$M_0 = \left(n_p - n_a\right)\mu_p \approx \frac{n\mu_p^2 H_a}{kT} \tag{48.53}$$

Once the fluid has reached equilibrium magnetization, the field is removed and the nuclei are allowed to precess about the local ambient field until they become randomized again. This process of excitation–relaxation can take as long as several seconds.

The hydrocarbon spin-lattice relaxation time can be adjusted by mixing paramagnetic salts, such as ferrous nitrate, into the solution. The trade-off in reduced relaxation time is increased signal-to-noise and resolution. Benzene is a good general-purpose hydrocarbon that can be used in a proton precession magnetometer.

Signal Conditioning

The block diagram shown in Figure 48.23 is an example of the signal conditioning required for a proton precession magnetometer. The coil surrounding the bottle containing the hydrocarbon serves two purposes. At the beginning of a measurement, the current source is connected to the coil to generate the magnetic field that polarizes the fluid. This field is on the order of 10 mT. After a few seconds, the current source is disconnected and the coil, which now has a decaying nuclear precession signal at its output, is connected to the input of the amplifier. The signal is amplified, filtered, and then the period of the Larmor frequency is measured, averaged, scaled, and presented to the user in magnetic field units on a digital display.

The scale factor of the proton precession magnetometer is based on the gyromagnetic ratio, which is 0.042579 Hz nT^{-1}. High resolution, up to 0.01 nT, is achieved by measuring the period of the signal rather than the frequency. The signal frequency can be divided down and used to gate a high-frequency oscillator that is driving a counter.

The sampling of the field is controlled manually in many commercially available proton precession magnetometers. Some magnetometers have an internally controlled sample rate. The sample rate and resolution are inversely related to one another. A higher sample rate produces a poorer resolution.

The Optically Pumped Magnetometer

As explained earlier, the optically pumped magnetometer is based on the Zeeman effect. This effect is most pronounced in alkaline vapors (rubidium, lithium, cesium, sodium, and potassium). Figure 48.24 is the hyperfine spectral structure for the valence electrons of rubidium (Rb) 85, which is commonly used in these types of magnetometers. The energy-related frequency interval between these hyperfine lines is proportional to the applied field. The magnetic quantum number m is related to the angular momentum number and specifies the possible component magnitude of the magnetic moment along the applied field. The optically pumped magnetometer takes advantage of this characteristic.

Transitions occur between levels of different m values and obey the rule that the change in m can only have the values 0, 1, and –1. Table 48.5 lists the relationship between the polarization of the light stimulating the transition and the allowable change in m.

When not optically excited, the energy states of the valence electrons will be distributed according to Boltzmann statistics and will be in a state of equilibrium. If the electrons are excited with circularly polarized light at the D1 frequency (794.8 nm wavelength), they will absorb photons and transition from the $^2S_{1/2}$ state to the $^2P_{1/2}$ state according to the transition rules. The excited electrons will then fall back in a random fashion to the lower states, being distributed with an equal probability among all the m states.

But the rules state that the change in m can only be 1 or –1 for polarized light. If one uses right circularly polarized light, then the change in m can only be 1, and the electrons in the m = 3 level of the $^2S_{1/2}$ state cannot transition since there is no m = 4 level at the $^2P_{1/2}$ state. Therefore, these electrons remain in the m = 3 state. All other electrons transition to the higher state and then fall back to the lower state

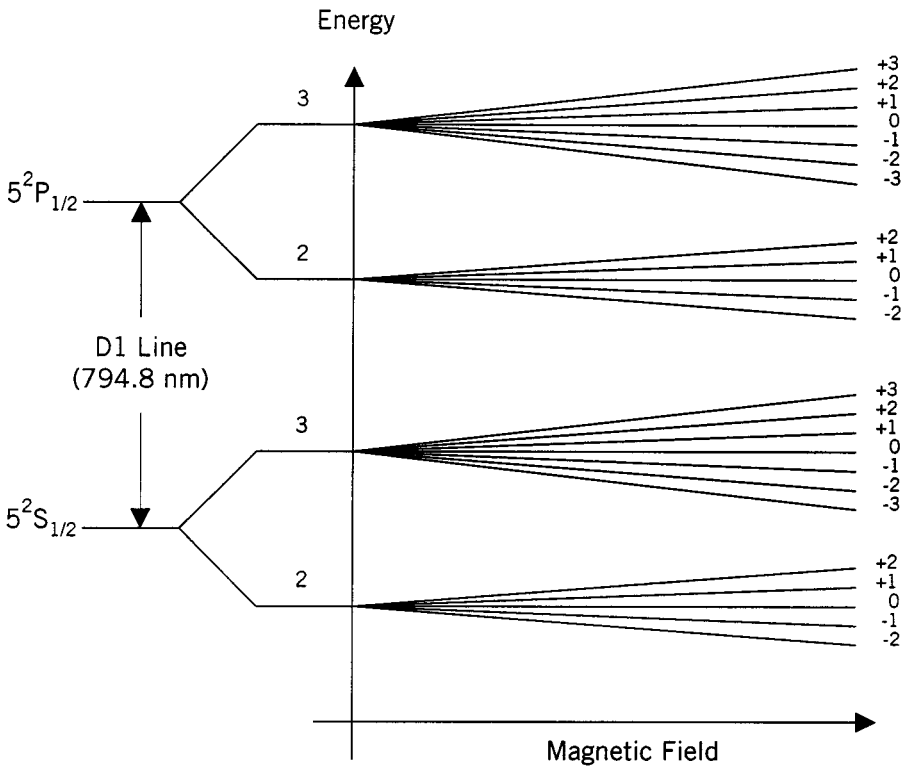

FIGURE 48.24 Rb-85 energy diagram. When a magnetic field is applied, the energy levels split into Zeeman sublevels that diverge as the field increases. Quantum mechanical factors determine the number of sublevels at each primary energy level.

TABLE 48.5 The Allowable Change in *m* When Jumping from One Energy Level to Another Depends on the Polarization of the Light Causing the Transition

Polarization	*m*
Left circular	–1
Parallel	0
Right circular	1

with equal probability of arriving at any of the *m* levels, including *m* = 3. Thus, the *m* = 3 level fills up, and the other levels empty until all the electrons are in the *m* = 3 level, and no more transitions to the higher state can take place. Pumping stops.

When pumping begins, the vapor is opaque. As time goes on, less electrons are available for absorbing photons, and the vapor becomes more transparent until, finally, pumping action stops and the vapor is completely transparent.

If a small RF magnetic field at the Larmor frequency is applied at right angles to the magnetic field being measured, the electrons in the *m* = 3 state will be depumped to the other *m* levels, making them available for further pumping. The optically pumped magnetometer exploits this situation in a positive feedback arrangement to produce an oscillator at the Larmor frequency.

The scale factors for optically pumped magnetometers are significantly higher than for the proton precession magnetometer. Table 48.6 lists these scale factors for a number of alkali vapors.

TABLE 48.6 The Change in Frequency for a Change in Field Is Much Higher in Optically Pumped Magnetometers Than in Proton Precession Magnetometers

Alkali	Scale factor (Hz nT^{-1})
Rb-85	4.66737
Rb-87	~7
Cesium	3.4986

As a result, the sample rate and resolution can be much higher. A resolution of 0.005 nT is possible. Sampling rates can be as high as 15 samples per second.

Signal Conditioning

Descriptions of several optically pumped magnetometers and their operating principles can be found in [24–26]. There are a number of different signal conditioning arrangements that can be used to derive a useful readout of the measured fields. Two of the more common methods are described in [26] and are shown in Figure 48.25.

In the servoed type shown in Figure 48.25(a), the magnetic field being measured and the RF field are coaxial. The frequency of the RF oscillator is modulated with a fixed low-frequency oscillator. This causes the RF frequency to sweep through the Larmor frequency. If the sweeped RF oscillator is not centered about the Larmor frequency, the photocell output signal will contain a fundamental component of the RF modulation frequency. The phase of the signal relative to the modulator oscillator determines whether the central RF frequency is above or below the Larmor frequency. The photocell output is phase-detected to produce an error voltage that is used to drive the RF frequency toward the Larmor frequency. The RF frequency can be measured to determine the magnetic field. If a linear voltage controlled oscillator is used as the RF oscillator, its control voltage can also be used as an output since it is a measure of the Larmor frequency.

The auto-oscillating type shown in Figure 48.25(b) is based on the transmission of a polarized beam that is at right angles to the field being measured. The intensity of this cross-beam will be modulated at the Larmor frequency. The photocell signal will be shifted by 90° relative to the RF field. By amplifying the photocell signal, shifting it 90° and feeding it back to drive the RF field coil, an oscillator is created at the Larmor frequency. In practice, only one light source is used, and the field being measured is set at an angle of 45°.

Defining Terms

Anisotropic: The material property depends on direction.

Gaussmeter: An instrument used to measure magnetic fields greater than 1 mT.

Induced magnetization: The object's magnetization is induced by an external magnetic field and disappears when the inducing field is removed.

Initial permeability: The slope at the origin of the magnetization curve.

Isotropic: The material property is the same in all directions.

Magnetic dipole moment: A vector quantity that describes the strength and direction of a magnetic field source, such as a small current loop or spinning atomic nucleus.

Magnetically "hard" material: The material has a significant residual (permanent) magnetization after an external magnetic field is removed.

Magnetically "soft" material: The material's magnetization is induced by an external magnetic field and the material has no significant residual (permanent) magnetization after the field is removed.

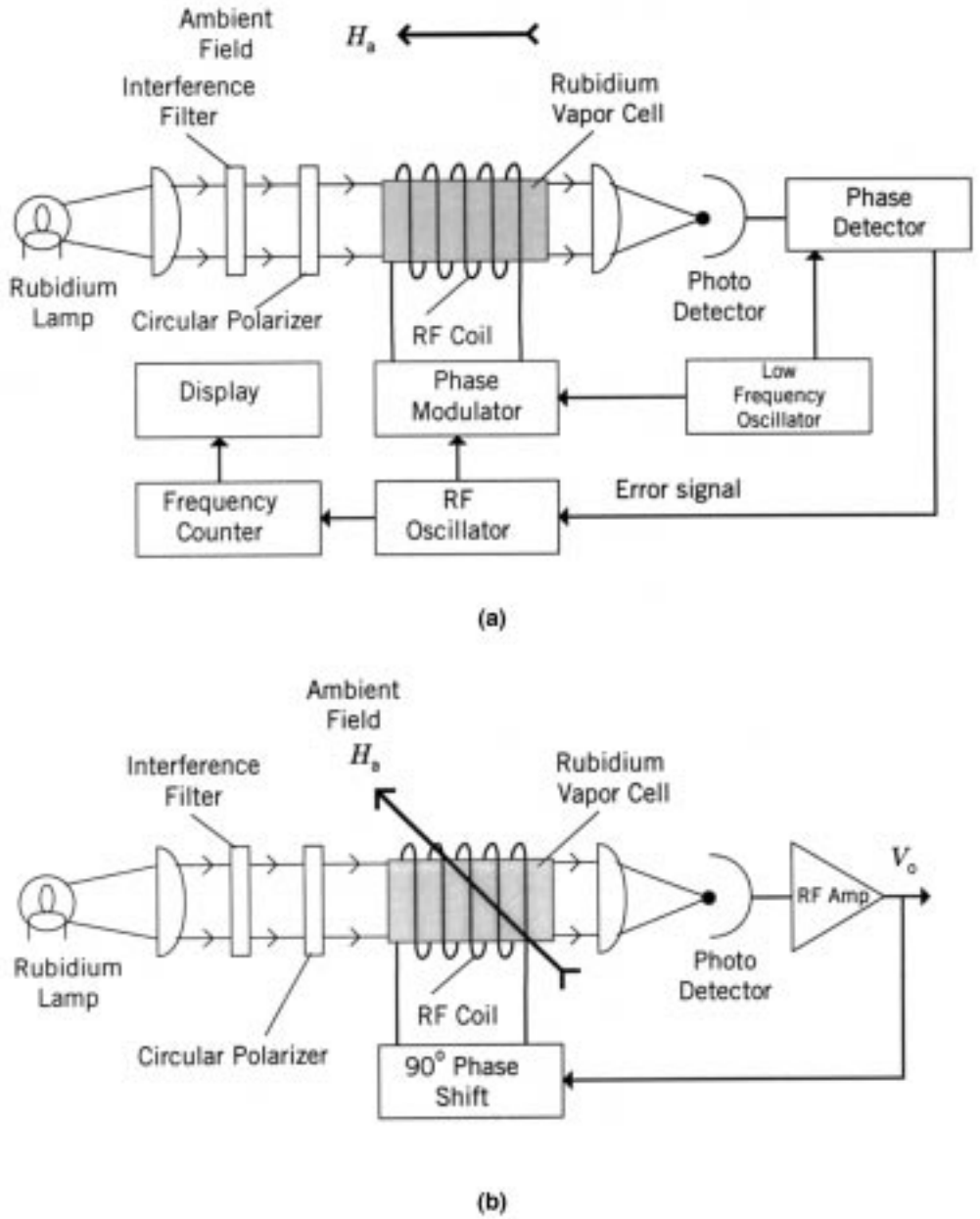

FIGURE 48.25 Two examples of optically pumped scalar magnetometers. The servoed magnetometer: (a) slightly modulates the RF field at a low frequency, causing the vapor transmissivity to modulate. A phase detector provides an error signal that is used to lock the RF oscillator to the Larmor frequency. (b) A self-oscillating magnetometer: the transmissivity of the vapor, at right angles to the applied field, is made to oscillate at the Larmor frequency by phase-shifting the detected light modulation and feeding it back to the RF field generator. (Adapted from Hartmann, 1972.)

Magnetization curve: A plot of flux density B vs. magnetic field H for an initially unmagnetized ferromagnetic material.

Magnetization: A vector quantity describing the average density and direction of magnetic dipole moments.

Magnetometer: An instrument used to measure magnetic fields with magnitudes up to 1 mT.

Magnetoresistance: The change in the electrical resistivity of a material in response to an applied magnetic field.

Maximum permeability: The maximum slope of the line drawn from the origin of the magnetization curve to a point on the magnetization curve.

Permanent magnetization: The source of an object's magnetization is internal and does not depend on the presence of an external field.

Permeability: A function that describes the relationship between an applied magnetic field and the resulting flux density.

Relative permeability: The permeability of a material normalized (divided) by the permeability of a vacuum.

Scalar magnetometer: A magnetometer that measures the magnitude of a magnetic field vector.

Vector magnetometer: A magnetometer that measures one or more of the individual components of a magnetic field vector.

References

1. K. S. Lion, *Instrumentation in Scientific Research. Electrical Input Transducers*, New York: McGraw-Hill, 1959.
2. H. R. Everett, *Sensors for Mobile Robots: Theory and Application*, Wellesley, MA: A. K. Peters, 1995.
3. J. E. Lenz, A review of magnetic sensors, *Proc. of IEEE*, 78, 973–989, 1990.
4. M. A. Payne, SI and Gaussian cgs units, conversions and equations for use in geomagnetism, *Phys. of Earth and Planitary Interiors*, 26, P10–P16, 1981.
5. F. W. Grover, *Induction Calculations. Working Formulas and Tables*, New York: Dover Publications, 1973.
6. R. M. Bozorth, *Ferromagnetism*, New York: D. Van Nostrand, 1951.
7. R. M. Bozorth and D. M. Chapin, Demagnetization factors of rods, *J. Appl. Phys*., 13, 320–326, 1942.
8. S. A. Macintyre, A portable low noise low current three-axis search coil magnetometer, *IEEE Trans. Magnetics*, MAG-16, 761–763, 1980.
9. J. P. Hauser, A 20-Hz to 200-kHz magnetic flux probe for EMI surveys, *IEEE Trans. Electromagnetic Compatibility*, 32, 67–69, 1990.
10. F. Primdahl, The fluxgate magnetometer, *J. Phys. E: Sci. Instrum*., 1, 242–253, 1979.
11. C. J. Pellerin and M. H. Acuna, A miniature two-axis fluxgate magnetometer, *NASA Technical Note*, TN D-5325, NASA, 1970.
12. S. V. Marshall, A gamma-level portable ring-core magnetometer, *IEEE Trans. Magnetics*, MAG-7, 183–185, 1971.
13. W. A. Geyger, *Nonlinear-Magnetic Control Devices*, New York: McGraw-Hill, 1964.
14. M. Acuna, C. Scearce, J. Seek, and J. Schelfiele, The MAGSAT vector magnetometer — a precise fluxgate magnetometer for the measurement of the geomagnetic field, *NASA Technical Report*.
15. D. Cohen, Measurements of the magnetic field produced by the human heart, brain and lung, *IEEE Trans. Magnetics*, MAG-11, 694–700, 1975.
16. C. M. Falco and I. K. Schuller, SQUIDs and their sensitivity for geophysical applications, *SQUID Applications to Geophysics*, The Society of Exploration Geophysicists, 13–18, 1981.
17. J. Clark, SQUIDs, *Sci. Am.*, 46–53, August 1994.
18. T. H. Casselman and S. A. Hanka, Calculation of the performance of a magnetoresistive permalloy magnetic field sensor, *IEEE Trans. Magnetics*, MAG-16, 461–464, 1980.
19. W. Kwaitkawski and S. Tumanski, The permalloy magnetoresistive sensors-properties and applications, *J. Phys. E: Sci. Instrum*., 19, 502–515, 1986.
20. Permalloy Magnetic Sensors, Honeywell Technical Note.
21. U. Dibbern and A. Petersen, The magnetoresistor sensor-a sensitive device for detecting magnetic field variations, *Electronic Components and Applications*, 5(3), 148–153, 1983.

22. S. Tumanski and M. M. Stabrowski, Optimization of the performance of a thin film magnetoresistive sensor, *IEEE Trans. Magnetics*, MAG-20, 963–965, 1984.
23. L. W. Parson and Z. M. Wiatr, Rubidium vapor magnetometer, *J. Sci. Instrum*., 39, 292–299, 1962.
24. W. H. Farthing and W. C. Folz, Rubidium vapor magnetometer for near Earth orbiting spacecraft, *Rev. Sci. Instrum*., 38, 1023–1030, 1967.
25. F. Hartmann, Resonance magnetometers, *IEEE Trans. Magnetics*, MAG-8, 66–75, 1972.
26. F. Wellstood, C. Heiden, and J. Clark, Integrated dc SQUID magnetometer with high slew rate, *Rev. Sci. Instrum.*, 66, 952–957, 1984.